RANS SIMULATION OF HYDROGEN FLAME PROPAGATION IN AN ACCELERATION TUBE: EXAMINATION OF k-ω SST MODEL PARAMETERS

Povilaitis, M.[1] and Jaseliūnaitė, J.[2]
[1] Laboratory of Nuclear Installation Safety, Lithuanian Energy Institute, Breslaujos g. 3, Kaunas, LT-44403, Lithuania, mantas.povilaitis@lei.lt
[2] Laboratory of Nuclear Installation Safety, Lithuanian Energy Institute, Breslaujos g. 3, Kaunas, LT-44403, Lithuania, justina.jaseliunaite@lei.lt

ABSTRACT

Due to practical computational resource limits, current simulations of premixed turbulent combustion experiments are often performed using simplified turbulence treatment. From all available RANS models, k-ε and k-ω SST are the most widely used. k-ω SST model is generally expected to be more accurate in bounded geometries, since it corresponds to k-ε model further from the walls, but switches to more appropriate k-ω model near the walls. However, k-ε is still widely used and in some instances is shown to provide better results. In this paper, we perform RANS simulations of premixed hydrogen flame propagation in an acceleration tube using k-ε and k-ω SST models. Accuracy of the models is assessed by comparing obtained results with the experiment. In order to better understand differences between k-ε and k-ω-SST results, parameters of main k-ω-SST model features are examined. The distribution of the blending functions values and corresponding zones of are analysed in relation to flame position and resulting observed propagation velocity. We show that, in the simulated case, biggest difference between k-ω-SST and k-ε model results can be attributed to turbulent eddy viscosity limiting by shear strain rate in the k-ω-SST model.

1. INTRODUCTION

Depending on the available computational resources and the size and complexity of studied domain, hydrogen turbulent combustion simulations can be performed with different level of details. In the most detailed case direct numerical simulation (DNS) is performed, which respectively requires the highest numerical resolution and computational resources. Consequently, DNS tends to be used for small scale simulation domains and detailed studies of physical phenomena. For larger simulation domains or with limited computational resource lower numerical resolutions need to be used. With lower resolutions comes the need to estimate turbulence parameters (instead of directly resolving) in parts of or whole computational domain. This leads to large eddy simulations (LES) or simulations employing Reynolds-averaged Navier–Stokes (RANS) equations. The latter requires less resources than LES, however it may provide less accurate turbulence estimation.

Lower resolution and resource requirements of RANS make them attractive for practical applications, especially when coupled with a simplified combustion model. It was established through a number of sequential international premixed turbulent hydrogen combustion benchmarks, that while there are areas requiring further improvements, generally RANS simulations were able to capture lean hydrogen-air mixture flame propagation in the case of obstacle induced turbulence [1-3].

k-ε [4] and k-ω-SST [5] turbulence models were the most widely used in these benchmarks. k-ω SST model is generally expected to be more accurate in bounded geometries, since it corresponds to k-ε model further from the walls, but switches to more appropriate k-ω model near the walls. However, k-ε model was more widely used and, in some instances, showed better results.

The aim of this paper is to better understand influence of different k-ω SST model components on the obtained results and origin of their differences from the k-ε results. We present RANS simulations of premixed hydrogen flame propagation in an acceleration tube using k-ε and k-ω SST models. Simulation results are compared with the experiments. In order to better understand k-ω SST model

operation and benefits compared to k-ε model, parametric variation of k-ω SST model parameters, separating it from k-ε model, is performed and result sensitivity is discussed.

2. METHODOLOGY

2.1. Experimental Facility

Experiment of hydrogen flame propagation in the acceleration tube, performed in ENACCEF facility [2] was simulated. ENACCEF facility is operated by (CNRS) in Orleans, France. The simulated experiment was originally performed for the SARNET2 hydrogen combustion benchmark [2].

In addition to a vertical acceleration tube, the ENACCEF facility also includes a wider dome situated at the upper exit of the tube. The height of elements are 3.3 m and 1.9 m, and their inner diameters are 154 mm and 726 mm, respectively. Furthermore, acceleration tube has nine annular obstacles with width of 2 mm. Obstacles are characterized by the blockage ratio:

$$BR = 1 - \left(\frac{d}{D}\right)^2 \tag{1}$$

where D – inner diameter of acceleration tube, m; d – inner diameter of obstacle, m.

First one is located at 0.638 m from the ignition point, further obstacles are continuously spaced 0.154 m apart. The mixture is ignited 0.138 m from the bottom of the facility using two thin tungsten electrodes connected to a high voltage source. Flame propagation was detected using 16 photomultipliers tubes and maximum pressure load was measured using 9 pressure sensors.

2.2 flameFoam solver

Simulations were performed with a CFD solver flameFoam version 0.8, developed for the premixed turbulent combustion. It is based on an open-source OpenFOAM toolbox [6] version 7. The solver source code is publicly hosted on https://github.com/flameFoam/flameFoam. The model is employed to solve unsteady Reynolds Averaged Navier-Stokes equations which are given as follows:

Mass conservation:

$$\frac{\partial \rho}{\partial t} + \Delta \cdot \left(\rho \vec{U}\right) = 0 \tag{2}$$

where ρ – density, kg/m^3; t – time, s; U – velocity, m/s.

Momentum conservation:

$$\frac{\partial \rho \vec{U}}{\partial t} + \Delta \cdot \left(\rho \vec{U} \times \vec{U}\right) = \nabla \cdot \tau_{eff} - \nabla p + \rho \vec{g} \tag{3}$$

where τ_{eff} – shear stress, N/m^2; p – pressure, Pa; g – gravitational acceleration, m/s^2.

Energy conservation:

$$\frac{\partial \rho h}{\partial t} + \Delta \cdot \left(\rho \vec{U} h\right) + \frac{\partial \rho K}{\partial t} + \Delta \cdot \left(\rho \vec{U} K\right) = \frac{\partial p}{\partial t} + \nabla \cdot \left(\alpha_{eff} \nabla h\right) + \rho\left(\vec{g} \cdot \vec{U}\right) + S_h(S_c) \tag{4}$$

where h - enthalpy, J; K – kinetic energy, J; α_{eff} – effective thermal diffusivity, m^2/s; S_h – enthalpy source, S_c – combustion source.

The propagation of flame front was modeled by employing a transport equation for the progress variable:

$$\frac{\partial \rho c}{\partial t} + \Delta \cdot \left(\rho \vec{U} c\right) = \nabla \cdot \left(\frac{\mu_{Eff}}{Sc_T} \nabla c\right) + S_c \quad (5)$$

where c – progress variable; μ_{eff} – effective dynamic viscosity, m^2/s.

Progress variable can have values between 0 – unburned mixture, and 1 – burned mixture. c is defined as:

$$c = \frac{Y_0^{H_2} - Y^{H_2}}{Y_0^{H_2} - Y_\infty^{H_2}} \quad (6)$$

where $Y_0^{H_2}$ – initial hydrogen mass fraction; Y^{H_2} – hydrogen mass fraction; $Y_\infty^{H_2}$ – final hydrogen mass fraction.

A progress variable transport equation is closed with the source term, which have form of turbulent flame speed combustion model:

$$S_c = \rho_u S_T |\nabla c| \quad (7)$$

where S_T – turbulent flame speed, m/s.

Turbulent flame speed was evaluated by Bradley correlation [7] from the following equation:

$$S_T = u' 0.88 \, (Ka \, Le)^{-0.3} \quad (8)$$

where u '– RMS velocity, m/s; Ka – Karlovitz stretch factor, Le – Lewis number.

Fluctuating velocity:

$$u' = \left(\frac{2}{3} k\right)^{\frac{1}{2}} \quad (9)$$

where k – turbulent kinetic energy, J/kg.

Karlovitz stretch factor:

$$Ka = 0.157 \left(\frac{u'}{S_L}\right)^2 Re_T^{\frac{-1}{2}} \quad (10)$$

$$Re_T = \frac{u' l_t^B}{\nu} \quad (11)$$

$$l_t^B = \left(\frac{3}{2}\right)^{\frac{3}{2}} \frac{u'^3}{\varepsilon} \quad (12)$$

where S_L – laminar flame speed, m/s; Re_T – turbulent Reynolds number; ν – kinematic viscosity, m^2/s; l_t^B – Bradley turbulent length scale, m; ε – turbulent dissipation rate, m^2/s^3.

Laminar flame speed is calculated using Malet's correlation [8]:

$$S_L = S_{L0} \left(1 - X_{H2_0}\right)^4 \left(\frac{T}{T_{ref}}\right)^{2.2} \left(\frac{p}{p_{ref}}\right)^{-0.5} \quad (13)$$

where S_{L0} – referential laminar flame speed, m/s; X_{H2_0}- initial steam volume fraction; T – temperature, K; T_{ref} – referential temperature, K; p_{ref} – referential pressure, Pa.

2.3 RANS models

k-ε [4] and k-ω-SST [5] turbulence models were used in the presented simulations. They are both two equation models, with k-ω-SST being composed of two dynamically zonally blended models – k-ε and k-ω. Two models are used since k-ω model is more suitable for wall bounded flows and k-ε for free stream flows.

The blending is realized using a blending function F_1:

$$\frac{\partial(\rho k)}{\partial t} + \frac{\partial(\rho U_i k)}{\partial x_i} = \widetilde{P_k} - \beta^* \rho k\omega + \frac{\partial}{\partial x_i}\left[(\mu + \sigma_k \mu_t)\frac{\partial k}{\partial x_i}\right] \quad (14)$$

$$\frac{\partial(\rho \omega)}{\partial t} + \frac{\partial(\rho U_i \omega)}{\partial x_i} = \alpha \rho S^2 - \beta \rho \omega^2 + \frac{\partial}{\partial x_i}\left[(\mu + \sigma_\omega \mu_t)\frac{\partial \omega}{\partial x_i}\right] + 2(1 - F_1)\rho \sigma_{w2}\frac{1}{\omega}\frac{\partial k}{\partial x_i}\frac{\partial \omega}{\partial x_i} \quad (15)$$

Model constants differing between the k-ε and k-ω are also appropriately blended using F_1 function.

$$F_1 = tanh\left\{\left\{min\left[max(A_{11}, A_{12}), \frac{4\sigma_{\omega 2} k}{CD_{k\omega} y^2}\right]\right\}^4\right\} \quad (16)$$

$$A_{11} = \frac{\sqrt{k}}{\beta^* \omega y} \quad (17)$$

$$A_{12} = \frac{500\nu}{y^2 \omega} \quad (18)$$

$$CD_{kw} = max\left(2\rho\sigma_{\omega 2}\frac{1}{\omega}\frac{\partial k}{\partial x_i}\frac{\partial \omega}{\partial x_i}, 10^{-10}\right) \quad (19)$$

where y – the distance to the nearest wall, m; $\sigma_{\omega 2}$ – model constant; β^* – model constant (0.09).

Away from the surface F_1 becomes zero and equation system (14-15) becomes equivalent to k-ε model. Inside the boundary layer F_1 switches to one and equation system (14-15) becomes equivalent to k-ω model.

However, there are more differences between the k-ε and k-ω-SST models in addition to blended equation system. In k-ε turbulent eddy viscosity is estimated from the expressions

$$\mu_T = \rho C_\mu \frac{k^2}{\varepsilon} \quad (20)$$

where C_μ – model constant (0.09).

While in the k-ω-SST this expression is complimented with a limiter based on an invariant measure of the strain rate S:

$$\nu_T = \frac{a_1 k}{max\,(a_1\omega, SF_2)} \quad (21)$$

F_2 is a blending function similar to F_1 used to activate the limiter only in the near-wall region:

$$F_2 = \tanh\left[\left[\max\left(\frac{2\sqrt{k}}{\beta^* \omega y}, \frac{500\nu}{y^2\omega}\right)\right]^2\right] \quad (22)$$

The third difference is turbulent kinetic energy production limiter intended to prevent the build-up of turbulence in stagnation regions:

$$P_k = min\left(\tau_{ij}\frac{\partial U_i}{\partial x_j}, c_1 k\omega\right) \quad (23)$$

where P_k – original production member from k-ε model; τ_{ij} – shear stress; c_1 – model constant, default value 10.

The result of these modifications is that k-ω-SST model operates in a zonal mode, with different zones of the domain having different turbulence models (k-ε, k-ω or a blend of two) and different expressions of turbulent eddy viscosity (conditionally on present strain rate). The distribution of the zones and model blends change dynamically depending on the actual conditions (blending functions F_1 and F_2).

2.4. Initial and boundary conditions

Initially the mixture is at rest at a temperature of 296.15 K and a pressure of 10^5 Pa. The initial hydrogen, steam and air distribution is homogenous and corresponds to concentration of 13 % H_2 and 30 % of H_2O. Lewis number for the mixture is selected to be 0.4. Thermophysical properties of the mixture were calculated using Cantera tool.

The boundary conditions are defined as no-slip adiabatic walls. For turbulence parameters standard boundary conditions were used, also initial values were selected as negligibly low values. Mesh was selected to have a 2D axisymmetric geometry (See Fig. 1). Grid is structured, uniform and has an element size of 1 mm, resulting in 877 069 cells in total. Ignition is modelled by setting circular area of ignition at the 0.138 m height in the middle of the facility with a burned mixture (c = 1). For transient simulations, a second order schemes were used for spatial discretization of all variables and Euler implicit scheme is employed for the temporal discretization.

To check grid sensitivity, simulations with a twice finer, 0.5 mm, mesh consisting of 3 511 676 cells were performed. Obtained results (Figs. 2 and 3) show very low result sensitivity to mesh change, especially in k-ε case. Due to low sensitivity, 1 mm mesh was used in the further simulations. The time step convergence was controlled by automatically varying time step to constrain the maximum Courant number below 0.35.

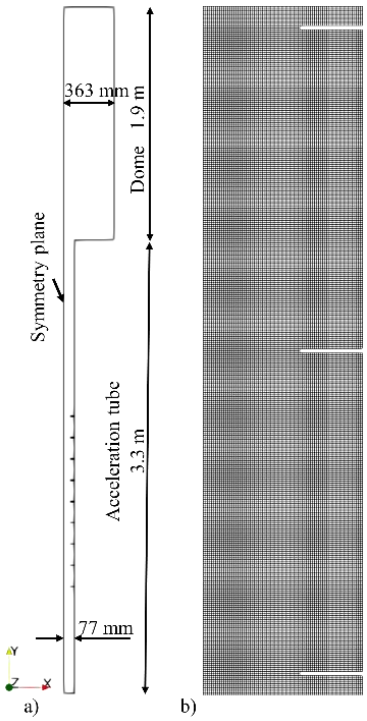

Figure 1. Geometry a) and mesh b) of computational domain

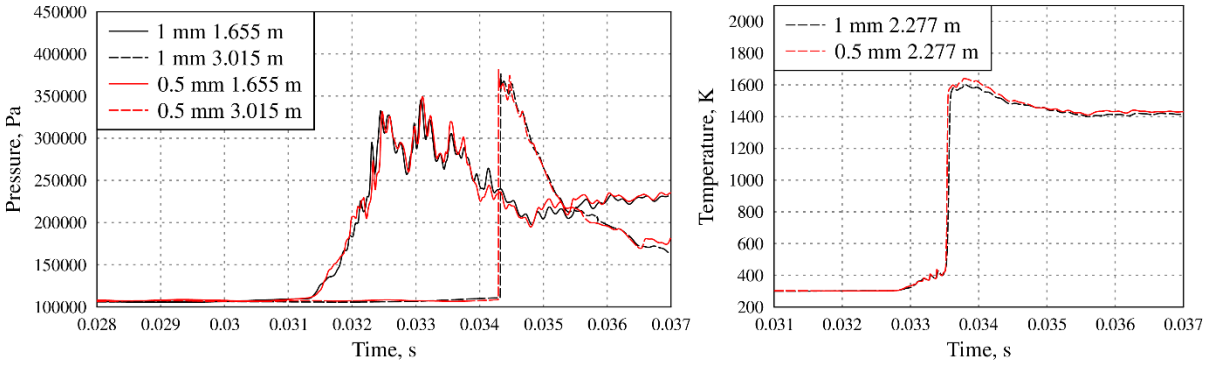

Figure 2. Comparison of pressure and temperature evolutions with different meshes (k-ε model)

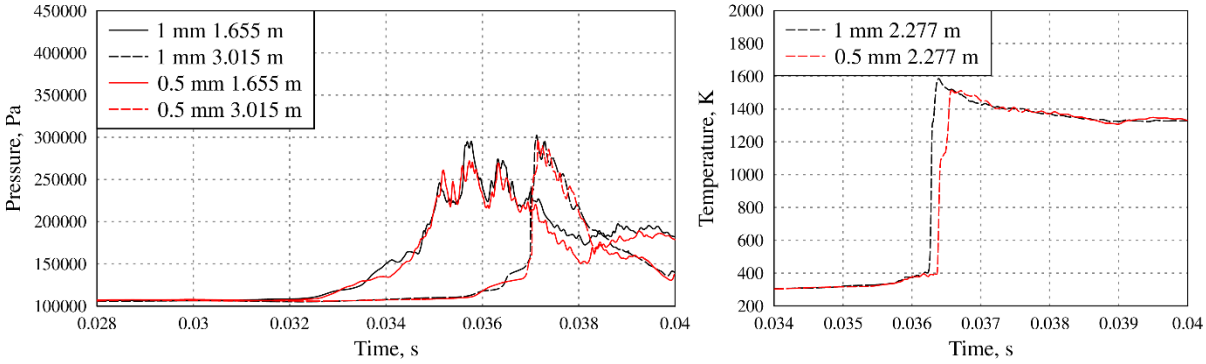

Figure 3. Comparison of pressure and temperature evolutions with different meshes (k-ω-SST model)

3. RESULTS AND DISCUSSION

Fig. 4 present comparison of experimental and numerical vertical observed flame velocity profiles. Numerical profiles obtained from calculations with k-ε and k-ω-SST RANS models are presented. Observed flame velocities were calculated from the flame arrival times using central difference estimation. Flame arrival in the simulations was assumed to correspond to the progress variable reaching 0.5 value.

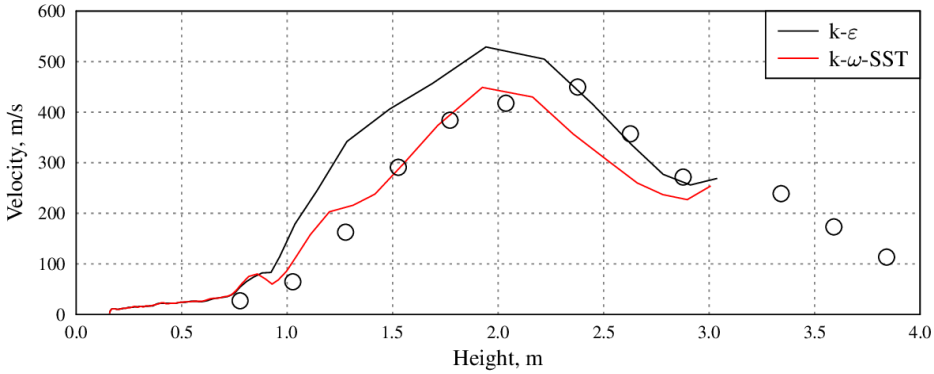

Figure 4. Experimental and numerical profiles of observed flame propagation velocity

After ignition at 0.138 m height flame propagates with low velocity until it encounters obstacles starting with 0.776 m height. Obstacle-induced turbulence accelerates the flame to 400 – 500 m/s velocity. Behind the obstacles turbulence level decreases and flame decelerates. At the exit to the dome turbulence is generated again, however in the experiment no acceleration was observed due to partial quenching. flameFoam does not model quenching process yet and increased turbulence would

result in incorrect prediction of flame propagation and second acceleration phase. Therefore, simulations were limited to the acceleration tube part of ENACCEF facility only as quenching process is out of scope for the present work.

Numerical results are similar with both used RANS models. However, k-ω-SST results align nicely with the experimental ones in the flame acceleration region, while k-ε shows over-prediction of velocity up to 100 m/s. With both RANS models velocity peak location was obtained at lower height compared to the experimentally observed.

In the deceleration phase k-ε calculations show better accuracy than k-ω-SST. Nevertheless, this deceleration is obtained starting from a higher, less accurate maximum velocity. The slope of deceleration aligns well with the experiment, indicating that k-ε model provided realistic simulation of turbulence decay in the flow behind the obstacles. However, k-ω-SST model provides similar deceleration slope as well. In both cases deceleration starts earlier (at lower height) compared to the experiment, indicating that initially turbulence is lost too rapidly and that later correspondence of k-ε and experiment decelerations might be resulting more from the fortunate combination of two errors – maximum velocity overestimation and earlier start of deceleration – than from the accurate simulation of actual transient. In k-ω-SST case only one of those two errors is present - earlier start of deceleration phase – unmitigated by other error it results in worse agreement.

Since the k-ω-SST results show good agreement with the experimental results until the underestimation of peak velocity location, it was decided to perform parametric analysis related to main components of the k-ω-SST model with the aim of better understanding obtained results and origin of the differences compared to k-ε results.

The variation of following parameters was performed:

1. Blending function F_1, which controls selection and blend between the k-ω and k-ε zones. However, in order to gain deeper insight, the value of F_1 was not varied directly. Instead, main two components of the hyperbolic tangent argument – A_{11} and A_{12} – were multiplied by additional constants C_{11} and C_{12}. In this way the hyperbolic tangent arguments could be scaled separately. With C_{11} and C_{12} both set to 0 k-ω-SST model would purely solve equation system equivalent to k-ε model.

2. Blending function F_2, which controls the calculation of turbulent eddy viscosity. The same approach as with F_1 was employed multiplying hyperbolic tangent arguments A_{21} and A_{22} with additional constants C_{21} and C_{22}.

3. Constant c_1 used to scale production limiter preventing the build-up of turbulence in stagnation regions.

These parameters cover the main three previously described features constituting k-ω-SST RANS model and distinguishing it from k-ε model – balance equation system, turbulent eddy viscosity expression and kinetic energy production limiter.

3.1 Blending function F_1

Fig. 5 shows influence of F_1 blending function (equation system) on the computed flame velocity profiles. In unmodified k-ω-SST calculation C_{11} and C_{12} are equal to one, $F_1 = 0$ case is obtained with zero C_{11} and C_{12}, and one intermediate case with twice smaller blending function arguments is provided as well.

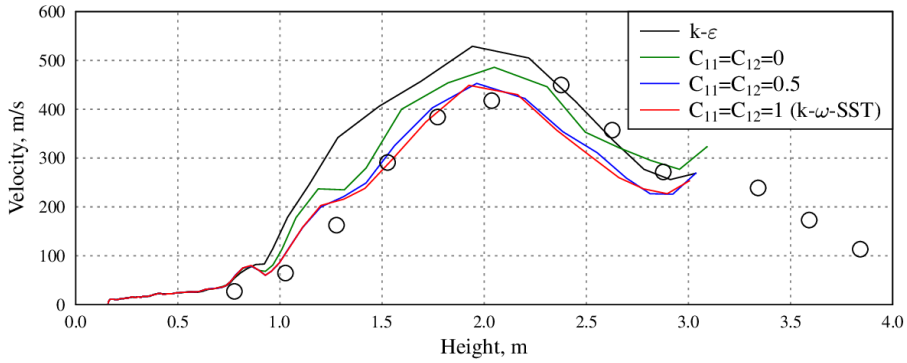

Figure 5. F_1 blending function impact on profiles of observed flame propagation velocity

Operating k-ω-SST model solely in the k-ε equivalent mode does not revert the results to the ones obtained from k-ε model. Results obtained with F_1 = 0 fall around the middle between k-ε and k-ω-SST results. It would seem as F_1 is responsible for an adequate part of the improvement in k-ω-SST results compared to k-ε model. Results with C_{11} and C_{12} set to 0.5 have no significant differences from the proper k-ω-SST model results. To examine such low sensitivity, Fig. 6 is presented, which shows flame position (black contour) and distributions of turbulent kinetic energy and F_1 blending function at selected time moments in C_{11} = C_{12} = 1 (proper k-ω-SST) and C_{11} = C_{12} = 0.5 (modified) cases. As expected, k-ω calculation zone (F_1 > 0.5) is extensive near the domain walls.

Fig. 6 shows that setting C_{11} = C_{12} = 0.5 has significant impact on F_1. At 35 ms in k-ω-SST case leading front of the flame is situated in the k-ω zone of the equations, while in the modified case in k-ε zone. However, 0.5 ms later where is no visible difference between the flames. This is explained by a low level of turbulence at this stage in the discussed location, consequently differences obtained from different k-ω-SST model regimes are inconsequential, and by the fact that k-ω zone extends more into the burnt mixture side from the flame than fresh. At 37 ms k-ω zone extension can be seen to be less further from the domain walls in modified case, resulting in more of the flame surface situated in k-ε zone. 0.5 ms later the impact of this can be seen at 1.15 m height with flame extended more in radial direction in modified case. While this does not significantly impact the axial propagation of the leading tip, the slight difference in the shape of leading front can be seen already, again due to faster radial propagation of flame in modified case. At 39 ms these differences are more pronounced. It can be seen that in modified case with wider k-ε zone general level of turbulence is higher, and consequentially flame is propagating slightly faster, especially in radial direction. However, the differences are too small to have an overall significant impact. And as Fig. 5 showed, even switching to k-ε zone in the whole simulation domain would produce mild impact.

In the context of k-ε RANS model, zonal switching to k-ω mode in k-ω-SST model seems to slightly suppress radial flame propagation (towards the walls) in the considered geometry and to generally decrease level of turbulence generated by the obstacles. However, the switching and blending of k-ε and k-ω zones (F_1 function) does not explain the whole difference between k-ε and k-ω-SST models, therefore it is also important to examine influence of the switching and blending of different turbulent eddy viscosity expressions (F_2 function).

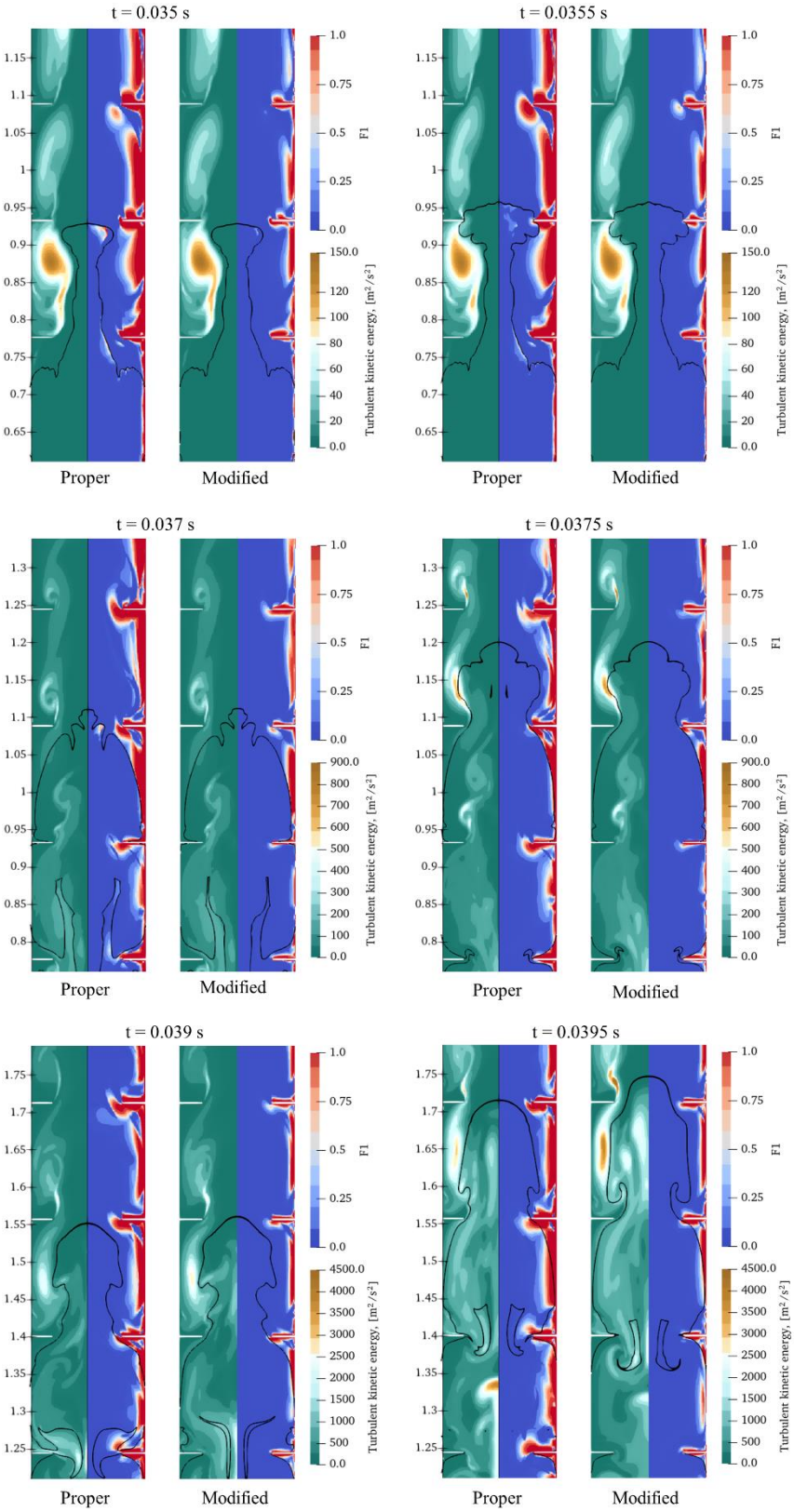

Figure 6. Comparison of flame position (black contour) and distributions of turbulent kinetic energy and F_1 blending function at selected time moments in $C_{11} = C_{12} = 1$ (proper k-ω-SST) and $C_{11} = C_{12} = 0.5$ (modified) cases

3.2 Blending function F_2

Influence of F_2 blending function on the computed flame velocity profiles is shown in Fig. 7. F_2 = 0 case is obtained with zero C_{21} and C_{22}, and one intermediate case with twice smaller blending function arguments is provided as well.

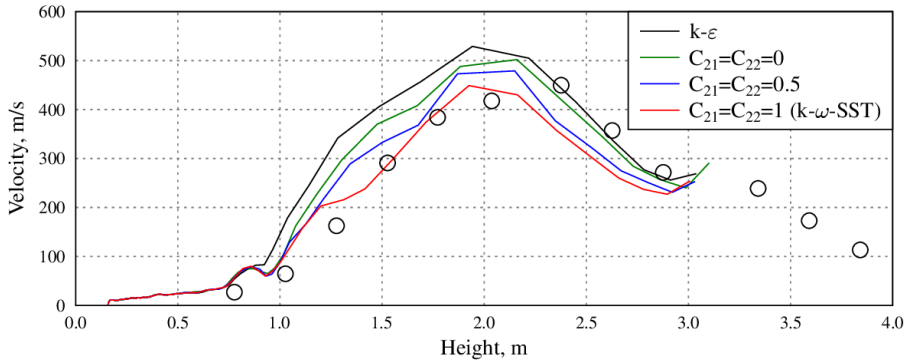

Figure 7. F_2 blending function impact on profiles of observed flame propagation velocity

Results obtained with F_2 set to zero are closer to the k-ε model results than with F_1 set to zero. Also, intermediate F_2 reduction has far more significant influence on the results than analogous intermediate reduction of F_1. This seems to imply that, in the studied case, used viscosity expression is more important to the obtained results than the used balance equation system.

To examine result sensitivity to F_2 function, Fig. 8 is presented, which shows flame position (black contour) and distributions of turbulent kinetic energy and F_2 blending function at selected time moments in C_{21} = C_{22} = 1 (proper k-ω-SST) and C_{21} = C_{22} = 0.5 (modified) cases. Since hyperbolic tangent arguments A_{12} and A_{22} are the same and A_{11} = A_{21}/2, F_2 distribution is, as expected, very similar to F_1 distribution, except higher F_2 zone extends further from the facility walls than F_1.

Impact of F_2 function variation on the results is more complex than of F_1 function. At 34 ms flame shapes are very similar in both cases. However high F_2 region extends less far from the domain walls in the modified case and consequentially there is significantly higher turbulent viscosity in the vortex region before the second obstacle. The resulting different vortex shapes and strength lead to diverging flame shapes, as can be observed 5 ms later. Vortex in unmodified case is able to pull flame more towards itself, expanding the leading flame finger. This difference of interactions occurs repeatedly, and flame shapes continue to diverge. At 35.5 ms in the proper k-ω-SST leading flame finger has already reached the obstacle and vortex before it, while in the modified case there is still a small gap between the flame and obstacles. 5 ms later both flames have backward propagating parts before the second obstacle, however in the proper k-ω-SST case this propagation is more advanced. This can be seen at 36.5 ms as well. Flame shape at 36.5 ms also shows that turbulent viscosity limiter used in k-ω-SST model tends to suppress formation of a tulip shape – in the modified case sides of the flame tend to propagate more in the axial direction than radial, forming shape closer to the tulip. 5 ms later this difference is even more visible. Due to the described influence of differences in turbulent viscosity model, with further propagation the flame shapes diverge far more significantly, leading to different flame propagation velocities as well.

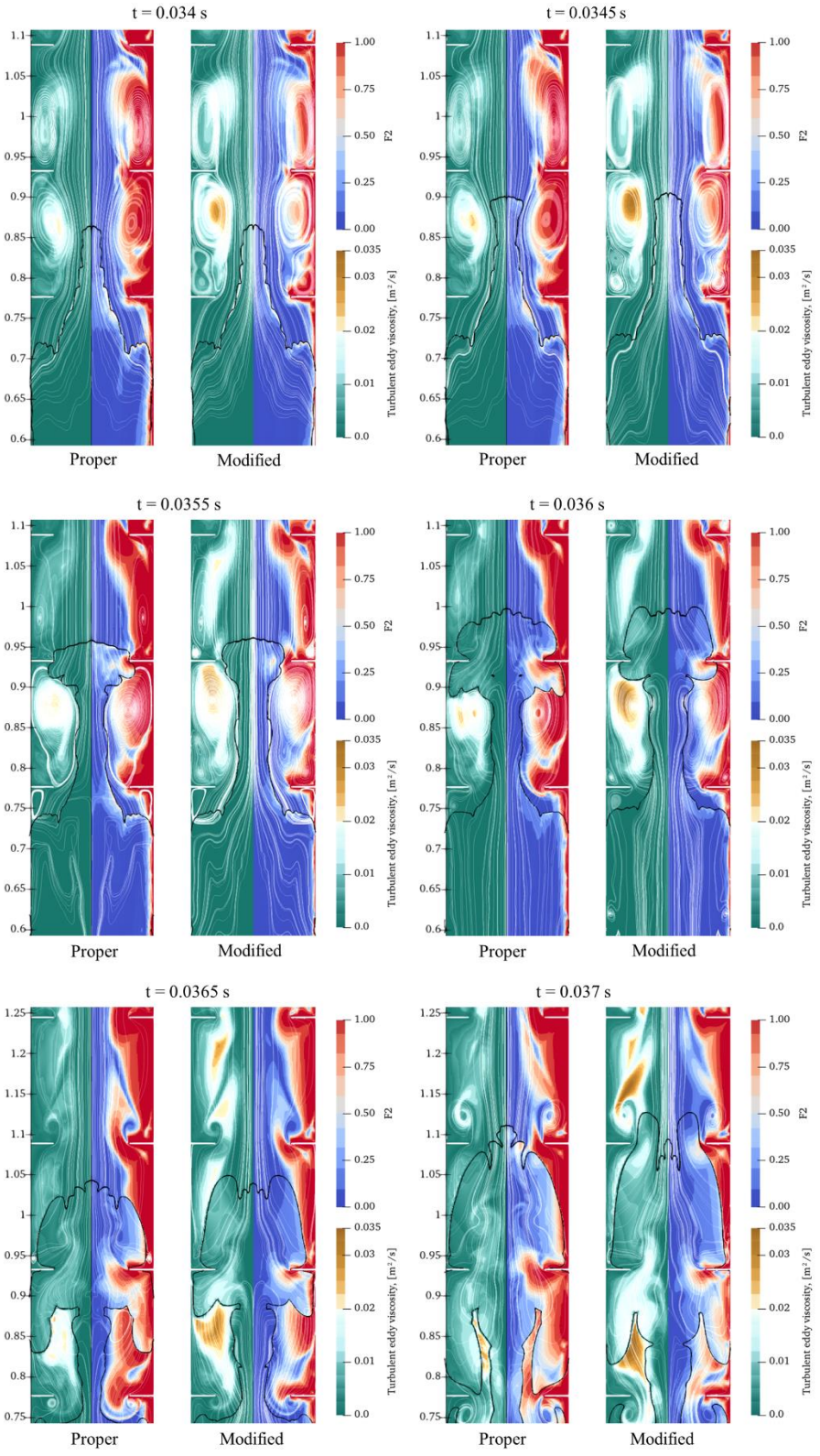

Figure 8. Comparison of flame position (black contour) and distributions of turbulent eddy viscosity and F_2 blending function at selected time moments in $C_{21} = C_{22} = 1$ (proper k-ω-SST) and $C_{21} = C_{22} = 0.5$ (modified) cases

Since F_2 function has a strong influence on the simulation results, it is interesting to examine impact of both its arguments separately. Fig. 9 presents obtained flame velocity profiles with only the A_{11} or A_{12} member turned off (respective constant C set to 0).

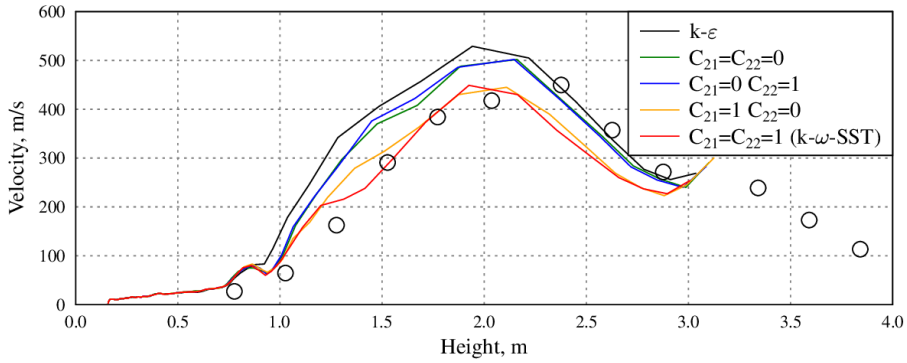

Figure 9. A_{21} and A_{22} impact on profiles of observed flame propagation velocity

It is clear that argument A_{11} is mostly responsible for the values of F_2 function in the studied case. Argument A_{12} was included in the k-ω-SST model to ensure that blending functions would not go to zero in viscous sublayer. It seems that in the simulated case this issue is insignificant for the overall flame propagation.

3.3 Production limiter constant c_1

In order to verify result sensitivity to turbulent kinetic energy production limiter, present in k-ω-SST model, multiplicative constant c_1 was varied. Default value of the constant is 10, increasing it raises the production limit (limiting becomes less strict). Fig. 10 presents flame velocity profile results obtained with different selected c_1 values. Increasing the constant 2 or 4 times moderately affects the observed flame velocity, mostly in the acceleration region. However, at higher values (increase by 8-10 times from the default) results become significantly sensitive, especially in the low turbulence region at the start of acceleration. In the deceleration region, where turbulence production is low, the limiter should be rarely activated even with low c_1 values and consequentially further coefficient increases should have no influence, which is reflected in similar velocity values in this region in all cases. The results confirm both the suitability of default c_1 value for the considered case, and low result sensitivity to the exact c_1 value close to the default.

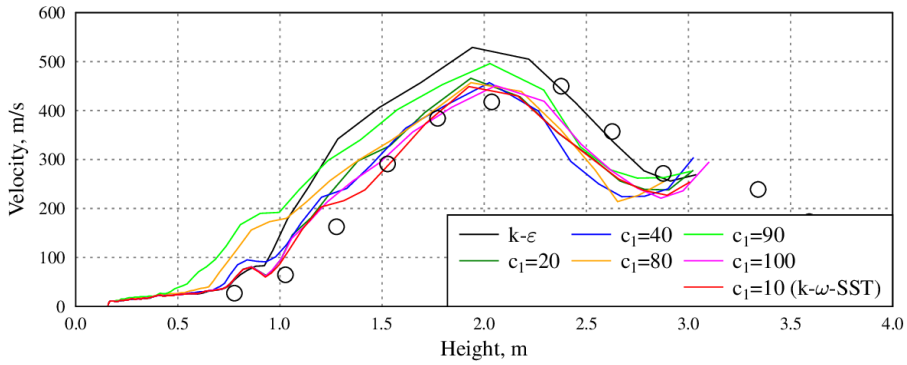

Figure 10. Production limiter impact on profiles of observed flame propagation velocity

CONCLUSIONS

Simulation of obstacle induced flame acceleration in 13% hydrogen – 30 % steam – air mixture was performed using RANS turbulence modeling and turbulent flame speed closure approach with Bradley correlation. Results obtained with k-ω-SST showed good agreement in the acceleration region, while k-ε model overpredicted turbulence and observed flame propagation velocity. Parametric analysis covering main features of k-ω-SST model was performed to better understand differences from k-ε results and impact of different k-ω-SST model components.

- The largest improvement of results compared to k-ε model came from the modifications to turbulent eddy viscosity. In k-ω-SST model eddy viscosity can be limited by high shear strain in near-wall regions (controlled by blending function F_2). Turbulent viscosities were indeed limited in the simulated case, impacting vortex shape and strength before obstacles and, through them, changing flame shape.

- With modified turbulent viscosity, flame front divergence to radial direction was promoted. Case with decreased F_2 function (weaker limit by shear strain) showed tendency for the sides of flame front to propagate axially and faster than centre of the flame resulting in tulip-like shape.

- Modifications to equation system of turbulence parameters (controlled by blending function F_1) had positive moderate influence on results.

- Limiting turbulent kinetic energy production is crucial to obtain accurate results during initial low-turbulence stage. Results are insensitive to the actual value of controlling coefficient c_1 in the range 10 – 40.

REFERENCES

1. International Standard Problem ISP-49 on Hydrogen Combustion, OECD NEA CSNI Final report NEA/CSNI/R(2011)9
2. Bentaib, A., Bleyer, A., Meynet, N., Chaumeix, N., Schramm, B., Höhne, M., Kostka, P., Movahed, M., Worapittayaporn, S., Brähler, T., Seok-Kang, H., Povilaitis, M., Kljenak, I. And Sathiah, P., SARNET hydrogen deflagration benchmarks: Main outcomes and conclusions, *Annals of Nuclear Energy,* **74**, 2014, pp. 143-152. https://doi.org/10.1016/j.anucene.2014.07.012
3. Bentaib, A., Chaumeix, N., Grosseuvres, R., Bleyer, A., Gastaldo, L., Maas, L., Jallais, S., Vyazmina, E., Kudriakov, S., Studer, E., Dehbi, A., Halouane, Y., Schramm, B., Taivassalo, V., Frankova, M., Kotsuba, O., Holler, T., Kljenak, I., Maruyama, Y., Nuri, T., Sato, M., Murgatroyd, J. and Povilaitis, M., ETSON-MITHYGENE benchmark on simulations of upward flame propagation experiment in the ENACCEF2 experimental facility, 12th International Topical Meeting on Nuclear Reactor Thermal-Hydraulics, Operation and Safety. Qingdao, China, Paper 776, 2018
4. Chien, K.-Y., Predictions of Channel and Boundary-Layer Flows with a Low-Reynolds-Number Turbulence Model, AIAA Journal, Vol. 20, No. 1, 1982, pp. 33-38.
5. Menter, F. R., Kuntz, M., and Langtry, R., Ten Years of Industrial Experience with the SST Turbulence Model, Turbulence, Heat and Mass Transfer 4, (K. Hanjalic, Y. Nagano, and M. Tummers Eds.), Begell House, Inc., 2003, pp. 625 – 632.
6. Weller, H.G., Tabor, G., Jasak, H. and Fureby, C., A tensorial approach to computational continuum mechanics using object-oriented techniques. Computers in Physics 12, 620, 1998
7. Bradley, D., Lau, A.K.C., Lawes, M. and Smith, F.T., Flame stretch rate as a determinant of turbulent burning velocity. Philosophical Transactions of The Royal Society A Mathematical Physical and Engineering Sciences 338, 359–387, 1992
8. Malet, F., Etude Expérimentale et Numérique de La Propagation de Flammes Prémélangées Turbulentes Dans Une Atmosphère Pauvre En Hydrogène et Humide. Ph.D. thesis. Université d'Orléans, 2005